Role of surface shape on boundary slip and velocity defect

Ali Dinler,[1,*] Robert W. Barber,[1] David R. Emerson,[1] Stefan K. Stefanov,[2] and Kamil Orucoglu[3]
[1]*Centre for Microfluidics and Microsystems Modelling, STFC Daresbury Laboratory, Warrington WA4 4AD, United Kingdom*
[2]*Institute of Mechanics, Bulgarian Academy of Sciences, Acad. G. Bonchev Str., Sofia 1113, Bulgaria*
[3]*Istanbul Technical University, Department of Mathematics, 34469, Maslak, Istanbul, Turkey*
(Received 15 February 2012; published 13 July 2012)

Although many gas-phase microfluidic devices contain curved surfaces, relatively little research has been conducted on the degree of slip over nonplanar surfaces. The present study demonstrates the influence of the surface shape (i.e., convex/concave) on the velocity slip and formation of the Knudsen layer. In addition, the study reveals that there is a simple relationship between the shear stress exerted on the surface and the velocity defect in the Knudsen layer.

DOI: 10.1103/PhysRevE.86.016314 PACS number(s): 47.61.Fg, 47.45.Gx

I. INTRODUCTION

The Knudsen layer extends just over one mean free path from a surface, and within this layer the momentum and heat transfer properties of the gas deviate considerably from the conventional continuum description of the fluid. The transport properties within the layer have been studied extensively for flows associated with planar surfaces [1–4]. The Knudsen layer manifests itself as a significant velocity defect (i.e., a deviation between the actual velocity profile and that predicted by the Navier-Stokes equations) in the near-wall region, and it is crucially important when modeling the flow behavior in gas-phase microdevices. The Knudsen number is defined as $\mathrm{Kn} = \lambda/L$, where λ is the mean free path of the gas molecules and L is the characteristic length scale of the flow. The Knudsen number, in fact, relates the thickness of the Knudsen layer to the length scale of the flow domain. As the Knudsen number increases, the Knudsen layer becomes increasingly influential on the flow behavior and causes a considerable velocity defect at any solid-gas interface.

The present study considers the flow of a rarefied gas driven by a thin rotating cylindrical shell positioned in the middle of the gap between two concentric stationary cylinders. The standard DSMC algorithm proposed by Bird [5] has been used with the exception of a small modification in the calculation of the maximum collision number in a cell, as described by Stefanov *et al*. [6]. In addition, a second-order slip model (the Navier-Stokes equations with slip boundary conditions) has been adopted for cylindrical surfaces. The velocity defect can be evaluated by comparing the difference between the normalized velocities from the slip solution with the results obtained from the direct simulation Monte Carlo (DSMC) solution. The present study highlights the profound role of the surface shape (i.e., whether the surface is convex/concave) on the flow behavior by specifically eliminating the effects of curvature and surface area. The study also demonstrates that anomalous velocity and temperature profiles appear in nonplanar geometries due to the surface shape.

*Author to whom all correspondence should be addressed: ali.dinler@stfc.ac.uk, ali_dinler@yahoo.com

II. THEORETICAL CONSIDERATION OF THE SHELL PROBLEM

In a cylindrical-polar coordinate (r,θ) reference frame, the circumferential momentum expression of the incompressible Navier-Stokes equations can be written as

$$\frac{d^2u}{dr^2} + \frac{d}{dr}\left(\frac{u}{r}\right) = 0, \tag{1}$$

where u is the velocity in the tangential direction and r is the radial distance. The general solution of Eq. (1) is given by

$$u(r) = C_1 r + \frac{C_2}{r}, \tag{2}$$

where C_1 and C_2 are constants determined by the slip boundary conditions.

Higher-order slip boundary conditions have great practical significance since they improve the accuracy of first-order slip models and extend the validity of the Navier-Stokes equations to higher Knudsen numbers. Several second-order slip models are proposed in the literature and their predictive capabilities have been the subject of many studies, as reviewed by Barber and Emerson [7] and Cao *et al*. [8]. Most of these boundary conditions, however, can only be applied to planar surfaces. To analyze the flow over cylindrical surfaces, we adopt a generic second-order slip boundary condition, formerly developed by Sone [9] for an arbitrary surface shape, and we express it by incorporating the Maxwell first-order slip boundary condition [10] as follows:

$$u_{\mathrm{slip}} = u_{\mathrm{gas}} - u_{\mathrm{wall}} = \pm A_1\left(\frac{2-\sigma}{\sigma}\right)\frac{\lambda}{\mu}\tau\Big|_{\mathrm{wall}} - A_2\frac{\lambda^2}{\mu}\frac{\partial\tau}{\partial n}\Big|_{\mathrm{wall}}, \tag{3}$$

where the subscripts "gas" and "wall" refer to the velocity of the gas and wall, respectively, σ is the tangential momentum accommodation coefficient, λ is the mean free path, μ is the dynamic viscosity, τ is the shear stress, $\partial/\partial n$ is the derivative in the direction normal to the surface, and A_1 and A_2 are the first- and second-order slip coefficients, respectively. The (viscous) mean free path is defined as $\lambda = (\mu/p)(\pi\mathcal{R}T/2)^{1/2}$, where p is the pressure, $\mathcal{R}$ is the specific gas constant, and T is the temperature. In the present study, the Knudsen number is defined in terms of the annular clearance between the shell and the confining inner (or outer) cylinder, i.e.,

 ©2012 American Physical Society

$\mathrm{Kn} = 2\lambda/(R_2 - R_1)$, where R_1 and R_2 are the radii of the stationary inner and outer cylinders, respectively.

The first-order term of the slip boundary condition in Eq. (3) was originally derived by Maxwell [10]. Subsequently, a second-order slip boundary condition for an arbitrary surface geometry was established by Sone [9,11] through a systematic asymptotic analysis of the Boltzmann equation and its boundary condition in half-space for small Knudsen numbers. In the case of isothermal flow between two concentric cylinders, Sone's second-order slip boundary condition can be cast in the form of Eq. (3), but it differs by the values of the first- and second-order coefficients. The $\pm$ sign in front of the first-order term in Eq. (3) is determined by the direction of the normal vector pointing into the gas. In this particular confined geometry, the direction of the normal vector at the inner cylinder is positive (r direction) while it is negative at the outer cylinder. The curvatures of the cylindrical surfaces also have opposite signs depending on whether the normal vector points toward the center of curvature or not; the curvatures of the convex and concave surfaces are positive and negative, respectively. This makes the magnitude of the second-order slip coefficient, A_2, in Eq. (3) identical at both the convex and concave surfaces with a minus ($-$) sign in front. In addition, it should be noted that the generic second-order boundary condition shown in Eq. (3) reduces to a form of a second-order slip boundary condition for planar surfaces, which has met with considerable success up to a Knudsen number as high as 0.4 [12–16].

The general solution of Eq. (1) for the concave and convex sides of the shell is obtained using the generic nonplanar boundary condition to give

$$\frac{u_{\mathrm{concave}}(r^*)}{\Omega R_S} = \frac{\Gamma_1(r_1) r_S^3 [r^*(r_S - r_1) + r_1]}{\Gamma_1(r_1) r_S^4 + \Gamma_2(r_S) r_1^4} - \frac{r_1^4 r_S^3}{[r^*(r_S - r_1) + r_1]\left[\Gamma_1(r_1) r_S^4 + \Gamma_2(r_S) r_1^4\right]}, \tag{4}$$

$$\frac{u_{\mathrm{convex}}(\hat{r})}{\Omega R_S} = \frac{\Gamma_2(r_2) r_S^3 [\hat{r}(r_2 - r_S) + r_S]}{\Gamma_1(r_S) r_2^4 + \Gamma_2(r_2) r_S^4} + \frac{r_S^3 r_2^4}{[\hat{r}(r_2 - r_S) + r_S]\left[\Gamma_1(r_S) r_2^4 + \Gamma_2(r_2) r_S^4\right]}, \tag{5}$$

where

$$\Gamma_1(r) = 4A_2 + 2A_1 r + r^2 \quad \text{and}$$
$$\Gamma_2(r) = -4A_2 + 2A_1 r - r^2, \tag{6}$$

and $r_1 = R_1/\lambda$, $r_S = R_S/\lambda$, and $r_2 = R_2/\lambda$ are the nondimensional radii of the inner cylinder, the shell, and the outer cylinder, respectively; $r^* = (r - R_1)/(R_S - R_1)$ and $\hat{r} = (r - R_S)/(R_2 - R_S)$ are the normalized radial distances for the concave and convex sides of the shell, respectively, and Ω is the angular velocity of the cylindrical shell. The slip coefficients in the present study are specified as $A_1 = 1.11$ and $A_2 = 0.61$ (following [12]) and the flow profiles are obtained for the fully diffusive case (i.e., $\sigma = 1$). The surface temperatures are assumed to be identical and specified as 273 K.

The present study implements the standard DSMC method proposed by Bird [5] for a cylindrical geometry but uses the modification detailed by Stefanov *et al.* [6] for the calculation of the maximum collision number in a cell. The DSMC method is a stochastic particle approach based on kinetic theory which can be shown to converge to the solution of the nonlinear Boltzmann equation in the limit of infinitesimal discretization if a sufficiently large number of particles is used in the simulation [17]. Each simulation particle in the DSMC method represents a large number of gas molecules, and therefore a relatively small number of particles is needed, which is an important advantage of the technique compared to molecular dynamics approaches. Another important feature of the DSMC method is that it is unconditionally stable. However, when the number of particles is small, the statistical noise increases considerably due to the fact that the collision term of the Boltzmann equation is simulated using random numbers based on the molecular chaos assumption of the collision process. The macroscopic properties of the gas (i.e., the physically observable quantities such as pressure and temperature) are postulated to be the averaged values of the microscopic random motion, and therefore the macroscopic quantities are calculated by averaging the microscopic values at the center of each cell.

In the present study, the gas behavior over the convex and concave sides of the shell has been simulated separately due to the two-part geometry of the shell problem. The simulations consider a hard-sphere model for argon at STP conditions and implement the Maxwell (specular-diffusive) gas-wall interaction model. Both flow domains over the concave and convex sides of the shell are divided into 200 cells in the radial direction, with each cell containing approximately 1000

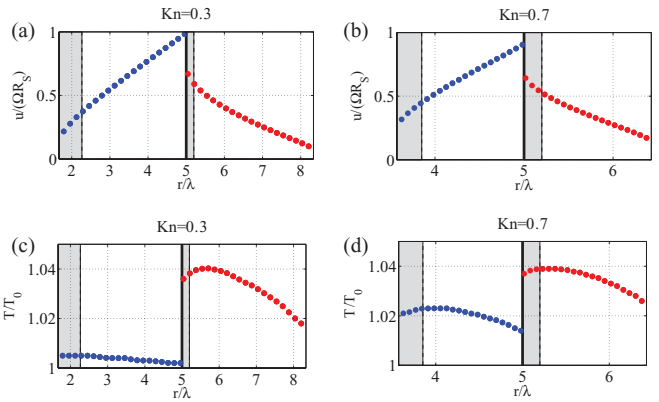

FIG. 1. (Color online) Comparison of velocity and temperature profiles over the concave and convex surfaces of a rotating cylindrical shell obtained using DSMC simulations. The shell is positioned midway between two stationary cylinders and has a radius of curvature of 5λ, where λ is the mean free path. The bold vertical lines in the middle of the figures represent the location of the shell while the shaded areas demonstrate the spatial extent of the S layers. The S layer extends from the convex surface by a distance of approximately $\lambda^2\kappa$ [18], where $\kappa = 1/\bar{r}\lambda^{-1}$ is the magnitude of the curvature of the convex surface and $\bar{r} = r_{\mathrm{convex}}/\lambda$ is the nondimensional radius of the convex surface.

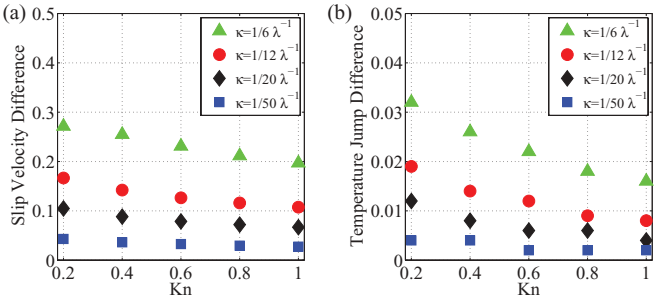

FIG. 2. (Color online) Difference in (a) slip velocities and (b) temperature jumps between the convex and concave surfaces of the shell. The radius of the shell is specified as 6λ, 12λ, 20λ, and 50λ, and the curvature κ is defined as the inverse of the magnitude of the shell radius. The slip velocities and temperature jumps are normalized by the velocity and temperature of the shell, respectively.

simulation particles on average. For the initial part of the study (shown in Figs. 1 and 2), the DSMC profiles have been obtained for a tangential wall velocity of 160 m/s (corresponding to a Mach number of ∼0.5). However, for the analysis of the velocity defect and formation of the Knudsen layer (Figs. 3 and 4), the DSMC data have employed a lower tangential wall velocity of 40 m/s (corresponding to a Mach number of ∼0.12). At this Mach number, the DSMC simulations show less than a 1% variation in density and temperature throughout the flow domain, demonstrating that compressibility and thermal effects are not important, and suggesting that our theoretical analysis shown above is valid.

III. VELOCITY SLIP AND THE FORMATION OF THE KNUDSEN LAYER

The anomalous velocity and temperature profiles for the rotating shell problem are presented in Fig. 1. The cylindrical shell is positioned in the middle of the annular gap and has a radius of curvature of 5λ, where λ is the mean free path. The bold vertical lines in the middle of the figures represent the location of the rotating shell, and the flows on the left- and right-hand sides of the shell are driven by concave and convex surfaces, respectively. The surfaces of the shell obviously have identical surface areas and equal magnitudes of curvature, and therefore any differences in the velocity and temperature

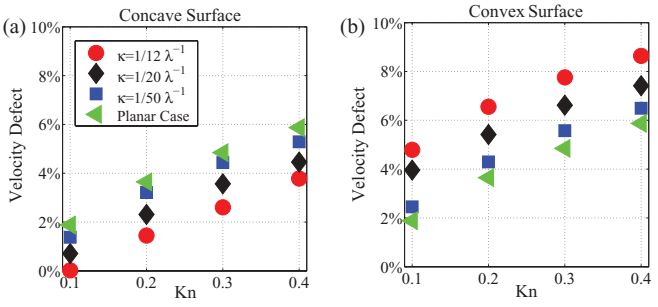

FIG. 3. (Color online) The effects of curvature on the velocity defect over concave and convex surfaces. The velocity defect is calculated as the difference between the normalized velocities obtained from the slip and DSMC solutions. (a) Velocity defect on the concave side, (b) velocity defect on the convex side of the shell.

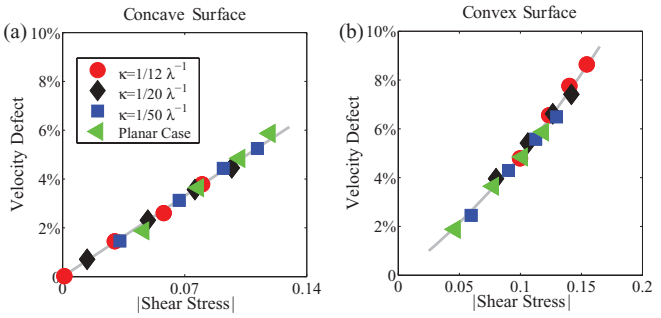

FIG. 4. (Color online) The velocity defect variation as a function of the magnitude of the nondimensional shear stress (a) at a concave surface and (b) at a convex surface. The shear stress exerted on the cylinder surface is obtained from the DSMC results. Identically shaped symbols from left to right represent the velocity defect at Knudsen numbers of 0.1, 0.2, 0.3, and 0.4, respectively.

profiles can be attributed to the effects of the surface shape (i.e., convex/concave) since the magnitudes of the slip and temperature jump would be equal on both surfaces in the equivalent planar flow problem. Figure 1 shows the remarkable differences in the slip and temperature jump on the concave and convex sides of the shell, and it highlights that the surface shape can have profound effects on the flow and temperature profiles over nonplanar surfaces.

Figures 1(a) and 1(b) show that the degree of slip over a convex surface is larger than that over a concave surface. This may be explained by the presence of the S layer over the convex surface; the S layer was originally described [18] as a "thin sublayer within the Knudsen layer," and its thickness was estimated to be of the order of $\lambda^2\kappa$, where κ is the magnitude of the curvature of the convex surface. However, the present results show that the influence of the S layer is rather significant. Furthermore, on the left-hand sides of Figs. 1(c) and 1(d), the temperature is shown to increase from the rotating concave surface to the stationary convex surface. These temperature profiles demonstrate a behavior that is analogous to the phenomenon of velocity inversion [19–21].

The variation of the slip velocity and temperature jump between the concave and convex sides of the shell is shown in Fig. 2 for different Knudsen numbers and different magnitudes of the shell curvature, κ. The radius of the shell is specified as 6λ, 12λ, 20λ, and 50λ. Figure 2 shows that both the slip velocity and the temperature jump differences increase with the magnitude of curvature, but interestingly, they decrease with the Knudsen number.

The Knudsen layer effects reveal themselves by a velocity defect at the solid wall which is the difference between the actual velocity of the gas molecules at the wall and the velocity predicted using a fluid-dynamic (Navier-Stokes) slip-flow description of the fluid. The velocity defect is obtained as a percentage using the formula

$$\text{velocity defect} = \left| \frac{u_{\text{DSMC}} - u_{\text{slip}}}{\Omega R_S} \right| \times 100, \qquad (7)$$

where u_{DSMC} and u_{slip} are the velocities at the wall obtained from the DSMC and the second-order slip model, respectively.

Figure 3 shows the effects of curvature on the velocity defect at a tangential wall velocity of 40 m/s (corresponding

to a Mach number of ∼0.12). Figure 3(a) demonstrates that the velocity defect over a concave surface decreases with curvature, whereas Fig. 3(b) shows that the velocity defect over a convex surface increases with curvature. This can be interpreted as an "opposing curvature effect" on the velocity defect over convex and concave surfaces. For a given Knudsen number, the velocity defect over the convex side of the shell is always larger than the velocity defect over the concave side. Moreover, the velocity defect for the equivalent planar flow case defines the effective upper and lower limits for the velocity defect over concave and convex surfaces, respectively.

Figure 4 demonstrates the important relationship between the magnitude of the nondimensional shear stress [i.e., $\tau^* = \tau\lambda/(\mu\,\Omega R_S)$] and the velocity defect over concave and convex surfaces. The relationship is linear over concave surfaces but exhibits a slight nonlinear trend over convex surfaces. A linear function of shear stress with a slope of 0.472 has been fitted to the velocity defect in Fig. 4(a) for concave surfaces. In this fit, the root mean square error (RMSE) is 0.000 25 and the coefficient of determination is 99.72%. Identically shaped symbols (for example circles) from left to right correspond to Knudsen numbers of 0.1, 0.2, 0.3, and 0.4, respectively. On the other hand, in the case of a convex surface, the relationship between the magnitude of the shear stress and the velocity defect is found to be

$$\text{velocity defect} = 0.37 \times |\text{shear stress}| + 1.2 \times |\text{shear stress}|^2, \tag{8}$$

where the RMSE is 0.001 65 and the coefficient of determination is 99.17%.

IV. CONCLUDING REMARKS

This study has highlighted the profound effect of the surface shape (i.e., whether the surface is convex/concave) on the velocity and temperature profiles in rarefied cylindrical Couette flow, and it has illustrated that the temperature profiles can exhibit anomalous behavior with the temperature increasing from a rotating concave surface to a stationary convex surface. This anomalous behavior can be explained by the role of the surface shape on the formation of the Knudsen layer. In addition, the study shows that the S layer, which is normally considered to be a thin sublayer within the Knudsen layer, can have a profound effect on the flow over convex surfaces.

The study has revealed that there is a remarkable relationship between the velocity defect within the Knudsen layer and the shear stress exerted on the flow surface. The results demonstrate that the formation of the Knudsen layer is markedly different over concave and convex walls. It is shown that the relationship between the shear stress and the velocity defect is linear over a concave surface but slightly nonlinear in the presence of the S layer over a convex surface.

Finally, the study has highlighted an important opposing effect of curvature on the velocity defect over concave and convex walls. A similar opposing effect on the velocity slip in liquid ^{3}He was proposed by Einzel *et al.* [22], who predicted a monotonic increase in the degree of slip at a convex surface, and conversely a monotonic decrease in the degree of slip at a concave surface, as the magnitude of the surface curvature increases. The direct simulation Monte Carlo results in the present study provide clear evidence that this opposing curvature effect on the velocity slip also occurs in rarefied gas flows over rotating cylindrical surfaces.

ACKNOWLEDGMENTS

The research leading to these results was funded by the European Community's Seventh Framework Programme (ITN-FP7/2007-2013) under the GASMEMS project (Grant Agreement No. 215504). The authors would also like to acknowledge support from the UK Engineering and Physical Sciences Research Council (EPSRC) under the auspices of Collaborative Computational Project 12 (CCP12).

[1] C. Cercignani, *Rarefied Gas Dynamics: From Basic Concepts to Actual Calculations* (Cambridge University Press, Cambridge, 2000).
[2] Y. H. Zhang, X. J. Gu, R. W. Barber, and D. R. Emerson, Phys. Rev. E **74**, 046704 (2006).
[3] J. M. Reese and Y. H. Zhang, J. Comput. Theor. Nanosci. **6**, 2061 (2009).
[4] X. J. Gu, D. R. Emerson, and G. H. Tang, Phys. Rev. E **81**, 016313 (2010).
[5] G. A. Bird, *Molecular Gas Dynamics and the Direct Simulation of Gas Flows* (Clarendon, Oxford, 1994).
[6] S. Stefanov, P. Gospodinov, and C. Cercignani, Phys. Fluids **10**, 289 (1998).
[7] R. W. Barber and D. R. Emerson, Heat Transf. Eng. **27**(4), 3 (2006).
[8] B. Y. Cao, J. Sun, M. Chen, and Z. Y. Guo, Int. J. Mol. Sci. **10**, 4638 (2009).
[9] Y. Sone, in *Rarefied Gas Dynamics*, edited by L. Trilling and H. Y. Wachman (Academic, New York, 1969), p. 243.
[10] J. C. Maxwell, Philos. Trans. R. Soc. London **170**, 231 (1879).
[11] Y. Sone, *Molecular Gas Dynamics: Theory, Techniques, and Applications* (Birkhäuser, Boston, 2007).
[12] N. G. Hadjiconstantinou, Microscale Thermophys. Eng. **9**, 137 (2005).
[13] C. Cercignani and S. Lorenzani, Phys. Fluids **22**, 062004 (2010).
[14] S. Colin, P. Lalonde, and R. Caen, Heat Transf. Eng. **25**, 23 (2004).
[15] I. A. Graur, P. Perrier, W. Ghozlani, and J. G. Méolans, Phys. Fluids **21**, 102004 (2009).
[16] P. Perrier, I. A. Graur, T. Ewart, and J. G. Méolans, Phys. Fluids **23**, 042004 (2011).
[17] W. Wagner, J. Stat. Phys. **66**, 1011 (1992).
[18] Y. Sone, Phys. Fluids **16**, 1422 (1973).
[19] K. W. Tibbs, F. Baras, and A. L. Garcia, Phys. Rev. E **56**, 2282 (1997).
[20] K. Aoki, H. Yoshida, T. Nakanishi, and A. L. Garcia, Phys. Rev. E **68**, 016302 (2003).
[21] S. Yuhong, R. W. Barber, and D. R. Emerson, Phys. Fluids **17**, 047102 (2005).
[22] D. Einzel, P. Panzer, and M. Liu, Phys. Rev. Lett. **64**, 2269 (1990).